JOURNAL OF MATERIALS SCIENCE 23 (1988) 2865–2870

Sintering and mechanical properties of ZrC–ZrO_2 composites

EUNGI MIN-HAGA*, WILLIAM D. SCOTT
Department of Materials Science and Engineering, University of Washington, Seattle, Washington 98195, USA

Zirconium carbide containing up to 40 wt% yttria-stabilized zirconia was sintered at 1800 to 2200° C in argon and carbon monoxide atmospheres in a graphite tube furnace. Well-dispersed fine powders containing 20 wt% ZrO_2 or more, when formed into compacts with green densities of 55% or above, could be sintered to theoretical density in 1 h at 2000° C. The resulting microstructure consisted of a dispersed ZrO_2 phase in a continuous zirconium oxi-carbide matrix. The fracture toughness and four-point bend strength were a maximum at 40 wt% ZrO_2 and were 5.8 MPa $m^{1/2}$ and 320 MPa, respectively. The fracture surface was irregular and primarily intergranular.

1. Introduction

Zirconium carbide is a member of the transition metal carbide family. It exhibits a high hardness and high melting point similar to other carbides such as WC, TiC, and TaC [1]. Single crystals of ZrC have been produced by the floating zone process [2] and small pellets of polycrystalline material were made by arc melting [3]. Barnier *et al.* [4] hot pressed ZrC at 40 MPa for 60 to 120 min at temperatures from 1700 to 2400° C. Densities which were 92.2% theoretical and above were obtained at 1900° C and above, with the maximum reported density being 6.43 g cm^{-3} (98.1%) after 60 min at 2300° C. Earlier hot-pressing work by Spivak and Klimenko [5] achieved densities of 92.5 to 94% at 200 kg cm^{-2} by sintering for 30 min at temperatures of 2200 to 2600° C, respectively.

Gropyanov and Bel'tyukova [6] sintered ZrC–ZrB_2 compacts and showed that the addition of 10% ZrB_2 enhanced the sintering of ZrC. They concluded that it was possible to obtain specimens with 2 to 4% porosity at 2027 to 2127° C using powders with specific surface area in the range 4 to 5 $m^2 g^{-1}$. Although total sintering times were 128 to 138 h, there was little change after 1 to 2 h.

Bulychev *et al.* [7] prepared sintered specimens of ZrC for mechanical properties tests using a carbon tube furnace in a hydrogen or argon atmosphere. At 2600° C, densities of about 98% were obtained after 60 min. However, at 2000° C and 60 min, the density was only 91% in argon and 93% in hydrogen.

As part of a larger study on the effects of additives on the sintering and strength of ZrC [8] it was observed that ZrC–ZrO_2 mixtures sintered quickly to near theoretical density and developed a well-dispersed two-phase microstructure. The purpose of the present work was to study the effects of various process parameters on the sintering and resulting microstructure of ZrC–ZrO_2 mixtures and to measure the mechanical properties of materials exhibiting promising microstructural characteristics.

Zirconium carbide has the NaCl structure and exists over a wide range of carbon deficient compositions [9]. ZrC can also incorporate oxygen into the structure, and Sarkar *et al.* [10] studied the relationship between oxygen concentration and the lattice parameter of zirconium oxicarbide. They found a linear decrease in a_0 from 0.469 80 to 0.4673 nm as the composition changed from $ZrC_{0.96}O_{0.04}$ to $ZrC_{0.69}O_{0.15}$. In the present work, the lattice parameter was measured as an indicator of the oxicarbide composition.

2. Experimental procedure

The raw materials used in this work are listed in Table I. Specimens will be designated as containing Type A or Type B ZrO_2 including the yttria content as shown in Table I. Type A was a pre-reacted yttria-stabilized zirconia with 3 mol % Y_2O_3. Type B was a physical mixture of ZrO_2 and Y_2O_3.

In the initial trials, ZrC and Type B ZrO_2 mixtures were ball milled up to 16 h in polyethylene mills using ZrO_2 balls. Although agglomerate particles were broken up, specimens which were slip cast, isostatically pressed and fired in argon were inhomogeneous and contained large pores as a result of polymer impurities introduced by the mill.

To avoid milling contamination and to eliminate large particles and agglomerates, particles below 1 μm were extracted from the as-received powder by sedimentation as follows. A suspension containing 172.8 g ZrC in 1000 ml H_2O (2.5 vol %) was adjusted to a pH 11.0 using NH_4OH. The suspension was subjected to ultrasonic agitation for 2 min using a 1.27 cm diameter probe. After dispersion the pH dropped to 10.5. The suspension was allowed to stand for 6 h and the upper

* *Present address:* Sumitomo Cement Company, Central Research Laboratory, Chiba, 174, Japan.

0022–2461/88 $03.00 + .12

TABLE I Raw materials analysis

ZrC*	ZrO_2		
	Oxide	Type A ZrO_2†	Type B ZrO_2‡
99% pure $ZrC_{0.97}$	ZrO_2	93.95	94.23
Total carbon: 11.4%	Y_2O_3	5.24	4.76
Free carbon: 0.2%	Al_2O_3	0.092	0.004
Av. particle size:	CaO	–	0.001
3.5 μm	Fe_2O_3	0.005	0.003
	MnO	–	0.001
	Na_2O	0.004	0.014
	SiO_2	0.011	0.013
	TiO_2	–	0.055
	SO_4	–	0.026
	Ig. loss	0.7	0.63
	Surface area ($m^2 g^{-1}$)	17	13.6
	Calc. size (nm)	24	75

*Furrchi Chemical Co., Tokyo, Japan.
†Toyo Soda Manufacturing Co., Tokyo, Japan.
‡Wah Chang Corp., Albany, Oregon, USA.

8 cm was carefully removed with a syringe. The pH of the separated portion was reduced to 9.7 by titration with HNO_3 and flocculation of the particles began in about 1 h. The clear supernatant was removed and the final process yield was 6.6 g or 3.8 wt %.

Although ZrC was well dispersed at pH 10.5, mixtures of ZrC and ZrO_2 (typically 0.75 ZrC, 0.25 ZrO_2 by weight) did not disperse at this pH. Fig. 1 shows the effect of PMAA additive and pH on the particle dispersion of pure ZrO_2. Additions of 0.5 wt % polymethacrylic acid ammonium salt PMAA followed by agitation for 2 min with the ultrasonic horn produced satisfactory suspensions of the ZrC–ZrO_2 mixtures as shown in Fig. 2. The mixtures required continuous stirring to maintain the dispersion. A final slurry containing more than 10 vol % solids was obtained by evaporation of the water at temperatures below 80° C while stirring slowly to avoid the introduction of air bubbles.

Test bars 6.8 mm wide × 110 mm long × 6.0 mm thick were cast on plaster blocks with impervious plastic side forms. The cast was allowed to go to completion, the side mould blocks removed, and the specimens were air dried for 12 h. Drying to constant weight was then done at 50° C over a period of about

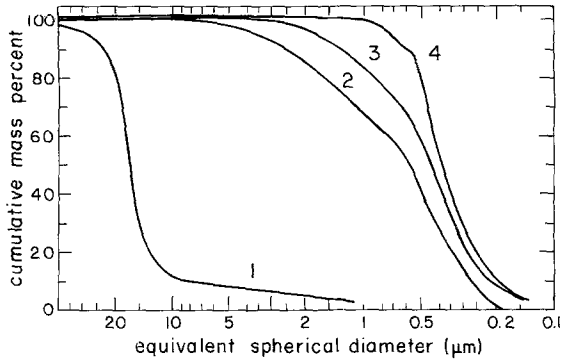

Figure 1 Effect of pH and PMAA dispersant on apparent particle size in ZrO_2 suspensions as measured by X-ray sedograph. (1) 0.0% PMAA, pH 9.5, (2) 0.25% PMAA, pH 9.5, (3) 0.25% PMAA, pH 10.0, (4) 0.5% PMAA, pH 10.0.

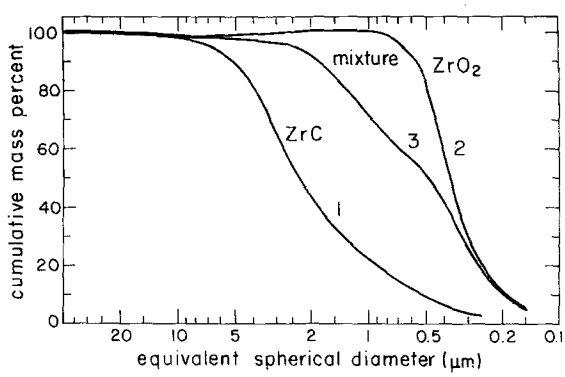

Figure 2 Dispersion curves for pure ZrC and ZrO_2 components and a mixture of 75 wt % ZrC–25 wt % ZrO_2. (1) ZrC, pH 9.8, (2) ZrO_2 with 0.5% PMAA at pH 10.0, (3) mixture of (1) and (2) at pH 10.0.

48 h. The cast specimens were cut and shaped by hand sanding into smaller bars about 5.4 × 35 × 4.47 mm.

Sintering was carried out in a graphite tube furnace in an argon atmosphere. Samples were placed in a graphite crucible and packed in loose powder of the same ZrC–ZrO_2 composition. The furnace was flushed with argon for 5 h to eliminate all oxygen, heated at 30° C min^{-1} to the desired sintering temperature, and held for 1 h. Temperatures were measured using an optical pyrometer sited on the side of the graphite crucible.

The apparent densities of the sintered samples were measured by water immersion. The specimens were prepared for microscopic examination by polishing on metal-bonded diamond wheels to 15 μm and finally on cloth laps using Al_2O_3 abrasives.

Flexural strengths were determined in four-point bending on 3.5 mm wide × 40 mm long × 3.0 mm thick bars at a cross-head speed of 0.2 mm min^{-1}, using an Instron testing machine. The outer span was 25.4 mm and the inner span was 12.7 mm. The tensile surface was finished with a 400 grit diamond wheel with the grinding passes parallel to the tensile axis. A chamfer on the corners of the tensile surface was made with a 15 μm diamond polishing wheel.

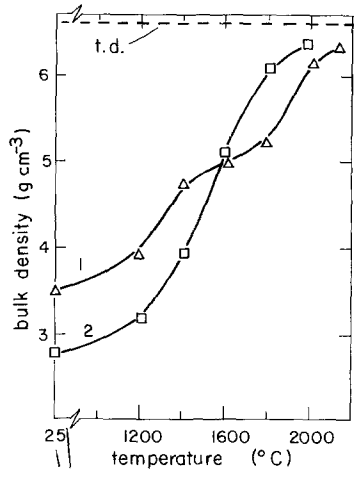

Figure 3 Density plotted against firing temperature for mixtures of 80 wt % ZrC, 20 wt % zirconia–yttria. (1) Type B ZrO_2 (see text), ball milled, and isostatically pressed. The particle size was < 2 μm. (2) Type A ZrO_2, dispersed using an ultrasonic probe at pH 10.0 with 0.5% PMAA, and slip cast. The particle size was < 1 μm. The green as-cast density is shown at 25° C.

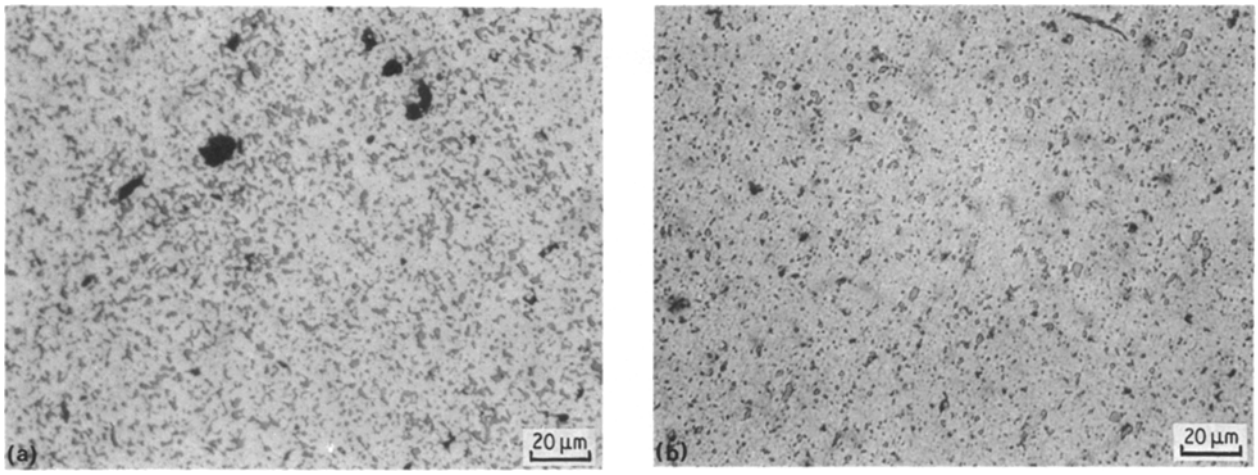

Figure 4 Optical micrographs of ZrC–ZrO_2 specimens fired at 2000° C for 1 h. The lighter phase is ZrC, and the darker phase is ZrO_2. The specimen in (a) corresponds to Curve 1 (Fig. 3) and (b) to Curve 2.

Fracture toughness was determined using the single notched beam method in three-point bending on the broken halves of the above strength specimens using a 12 mm span and the 3.5 mm dimension in the thickness direction. The following equation was used to calculate the fracture toughness [11]

$$K_{IC} = 3YPsa^{1/2}/2bw^2$$

where P is the breaking load, a the notch depth, b the specimen width, w the specimen depth, s the outer span, and Y a dimensionless parameter given by $Y = A_0 + A_1(a/w) + A_2(a/w)^2 + A_3(a/w)^3 + A_4(a/w)^4$. The values of the coefficients A_i depend on s/w (~ 4), and the corresponding values of the coefficients were: 1.93, −3.07, 14.53, −25.11, 25.80 [11]. The crosshead speed for the fracture toughness tests was 0.05 mm min^{-1}. The notch was cut with a 0.15 mm thick diamond wheel and the ratio of a/w was about 0.3.

3. Results and discussion

Fig. 3 shows the results for bulk density against firing temperature for two types of mixture containing 80% ZrC and 20% ZrO_2. Curve 1 is for ball-milled mixtures containing Type B ZrO_2 which were isostatically pressed to a green density of 58%. The powder used to prepare the specimens for Curve 2 was obtained by sedimentation and was $< 1\ \mu m$ in size. The ZrO_2 was Type A and contained 3 mol % Y_2O_3 as a dopant. Specimens were slip cast with no subsequent pressing, and the starting density was rather low, 45% theoretical (see Section 2). However, sintering occurred more rapidly than in Case 1 and the final density value of 95% was achieved at a temperature more than 100° C lower than for Curve 1.

The microstructures of the two types of specimens after firing for 1 h at 2000° C are shown in Figs 4a and b. The specimens made by dispersion and slip casting had a more uniform two-phase microstructure and fewer pores than specimens prepared by milling and pressing.

There was significant weight loss of the specimens during firing. Fig. 5 shows the high-temperature portion of a sintering curve for a mixture containing 30 wt % Type A ZrO_2 (dispersed and cast) and the associated weight loss. It was observed in the microstructures that ZrO_2 was either disappearing by vaporization or reacting to form ZrC or both. If all the ZrO_2 in a 30% mixture was converted to ZrC, the weight loss would be 4.87%, assuming the carbon came from a source external to the specimen. The weight loss approaches 5.5% at 2200° C and the microstructure showed that a large amount of ZrO_2 remained. Therefore, there must have been some evaporation of the oxide.

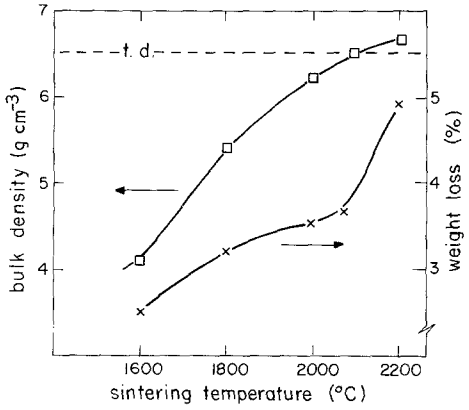

Figure 5 Weight loss and density of a mixture containing 30 wt % Type A ZrO_2 after 1 h sintering at various temperatures. The specimens were prepared by dispersion and slip casting.

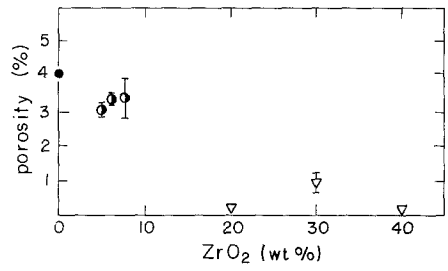

Figure 6 The effect of ZrO_2 content on residual closed porosity after firing for 1 h. The high data point at 30 wt % ZrO_2 is attributed to low green state density. (◑, ●) Specimens containing Type B ZrO_2, ball milled and pressed. (▽) Type A ZrO_2, dispersed and cast. (▽) 2000° C, (◑) 2200° C, (●) 2400° C.

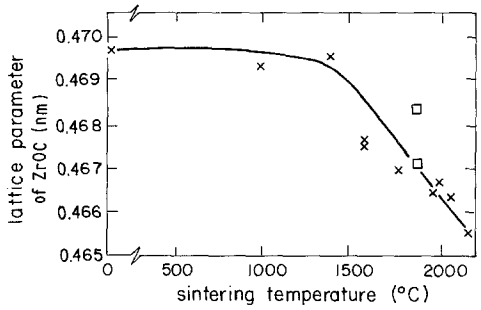

Figure 7 Decrease of ZrC lattice parameter with increasing firing temperature for specimens similar to those of Fig. 5. From the work of Sarkar *et al.* [10] this decrease indicates an increasing oxygen content in a Zr–O–C compound. (□) Sintering in a CO atmosphere.

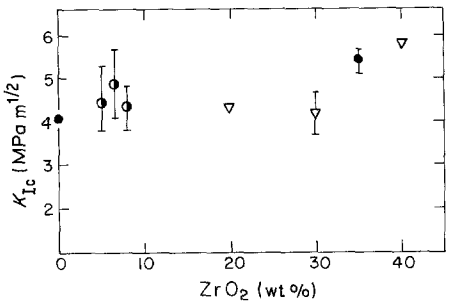

Figure 9 Fracture toughness measured by notched beam technique increases with increasing zirconia content, reaching a maximum value of 5.8 MPa m$^{1/2}$ at 40 wt % Type A zirconia addition. For key, see Fig. 6.

Fig. 6 gives the results for the effect of ZrO_2 content on residual closed porosity after firing for 1 h. At 20 wt % ZrO_2 and above, the porosity was reduced to below 0.2% provided the green-state processing was optimized.

The zirconia used in the present work contained yttria. X-ray diffraction analysis showed only the cubic form up to 15% ZrO_2, but above this value there was an increasing fraction of retained tetragonal phase until at 40% addition about one-fifth of the zirconia was retained tetragonal.

The ZrC phase was unchanged up to 1500° C but, as shown in Fig. 7, above this temperature there was a decrease in the lattice parameter with increasing firing temperature. This behaviour is consistent with the results of Sarkar *et al.* [10] for the formation of a Zr–O–C compound at 1800° C from mixtures of ZrO_2 and carbon. The smallest lattice parameter obtained by them was 0.407 nm for a composition $ZrC_{0.75}O_{0.148}$. This is approximately the same value shown in Fig. 7 for 1800° C. However, in the present work, the lattice parameter decreased further at higher temperatures. From an extrapolation of their results, the lowest a_0 in Fig. 7 would correspond to $ZrC_{0.75}O_{0.21}$.

Figs 8 to 10 summarize the strength, fracture toughness and hardness results. The strength in four-point bending increased from 220 to 320 MPa with increasing zirconia content, while the fracture toughness increased from about 4 to 5.8 MPa m$^{1/2}$ at 40 wt % Type A zirconia. Watanabe and Shoubu [12] formed dense TiB_2–ZrO_2 composites with 25 to 75 wt % ZrO_2 by hot pressing. They found that K_{IC} values increased from 4 to a maximum of 8 MPa m$^{1/2}$ in going from 20 to 40 wt % ZrO_2 while the transverse rupture strength increased from 350 to 750 MPa. The improvement in mechanical properties was attributed to the formation of partially stabilized ZrO_2 and $(TiZr)B_2$ solid solution.

In the present work the observed increase in fracture toughness and strength may be attributed to the presence of tetragonal ZrO_2. However, another possibility is the presence of residual stress in the two-phase microstructure.

The thermal expansion coefficient (TEC) of cubic ZrO_2 is 11 × 10^{-6} °C^{-1} while the TEC for ZrC is anisotropic and is 4.7 to 6 × 10^{-6} °C^{-1}. As the compact cools from the sintering temperature, the ZrO_2 will be placed in tension and the ZrC in compression. Several authors have considered the effects of thermal expansion mismatch in a particulate composite on the generation of microcracks and the subsequent effects on the mechanical properties. In most cases the dispersed particulate phase has a lower TEC than the matrix which produces matrix microcracks on cooling [13].

The opposite case in which the particulate material has a higher TEC than the matrix has been investigated for composites of Si_3N_4–SiC [14, 15], SiC–ZrO_2 [16], and SiC–TiC [17]. With the exception of the last system, there was a degradation or only a modest improvement in fracture toughness and strength with increasing second-phase content. In the SiC–TiC system, the improvement in mechanical properties was attributed to crack deflection.

Fig. 11 is a transmission electron micrograph of a ZrO_2 grain in the ZrC matrix, and shows the coherent

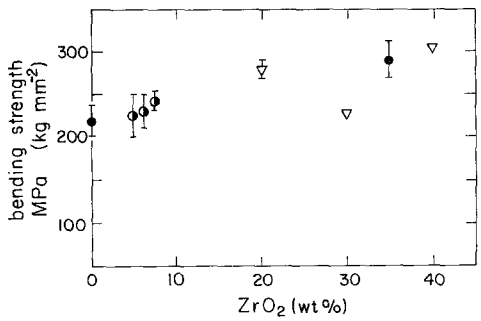

Figure 8 Tensile strength in four-point bending. There is a modest increase in strength with increasing zirconia content. The symbols refer to the same conditions as shown in Fig. 6.

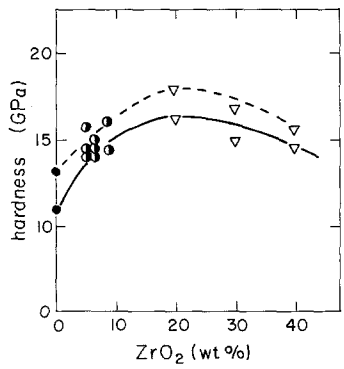

Figure 10 The Vickers hardness as a function of zirconia content. The pure ZrC material contained 4% residual porosity. (– – –) Vickers hardness, (——) Knoop hardness. For key, see Fig. 6.

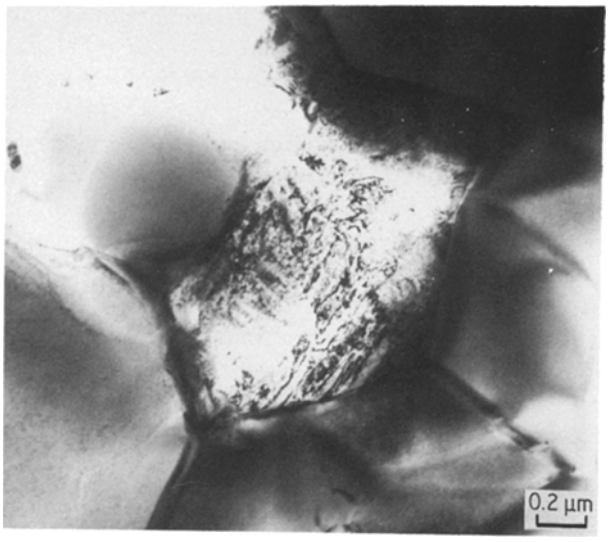

Figure 11 Transmission electron micrograph of a ZrO_2 grain in the ZrC matrix. The texture in the ZrO_2 is thought to be tetragonal precipitates and is the subject of further investigation.

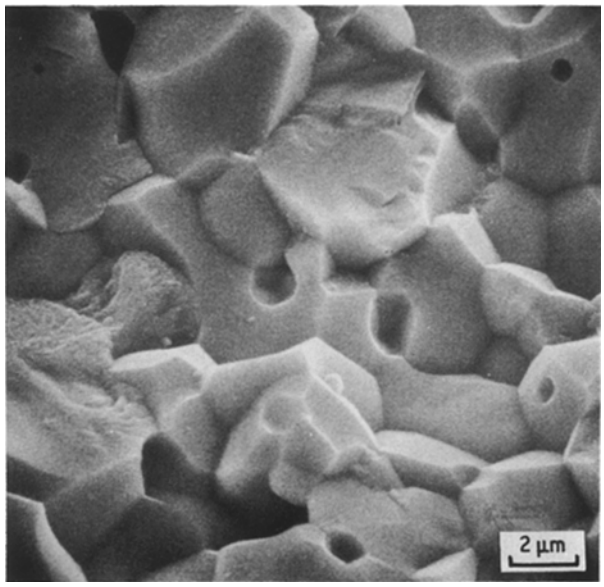

Figure 13 Scanning electron micrograph of the fracture surface of a notch beam fracture toughness specimen. The fracture path is mainly intergranular.

ZrO_2–ZrC interface, the well-sintered ZrC structure and the equilibrium triple-point angles established between the ZrO_2 and ZrC phases. No microcracks in or around the ZrO_2 were observed in the TEM specimens. As the ZrO_2 phase is expected to be in tension, the crack deflection model rather than the microcrack model is probably appropriate. Fig. 12 shows a typical crack pattern from a hardness indentation with crack branching and deflections and Fig. 13 confirms the intergranular fracture path.

Using the measured fracture toughness values (Fig. 9), the observed strengths correspond to a calculated critical flaw size of about 300 μm. This is much larger than the typical grain structure of the composite and indicates that the strength is controlled by singular processing defects. Pores were often observed in the vicinity of ZrO_2 grains, especially after prolonged heating. It was concluded that the ZrO_2 continued to react with carbon or ZrC to form oxicarbide with an associated reduction in molar volume of 9%.

The reaction of ZrO_2 was further demonstrated during annealing experiments intended to increase the tetragonal fraction of the zirconia phase. After a second heat treatment in argon in the carbon tube furnace for 1 h at 1800° C, a 50 μm thick layer of the surface of the composite was completely converted to ZrC, and after this surface layer was removed by polishing, the specimen density was found to be reduced.

The ZrO_2 reduction could be by the reaction

$$ZrO_2 + 3C = ZrC + 2CO \quad (1)$$

with the equilibrium being established through the carbon heating element of the furnace. Thermodynamic calculations show that the equilibrium pressure of carbon monoxide is 2 atm at 1727° C, so this reaction will proceed to the right in a system with flowing argon and a carbon heating element.

In an attempt to control the reduction of ZrO_2, some sintering runs were carried out in carbon

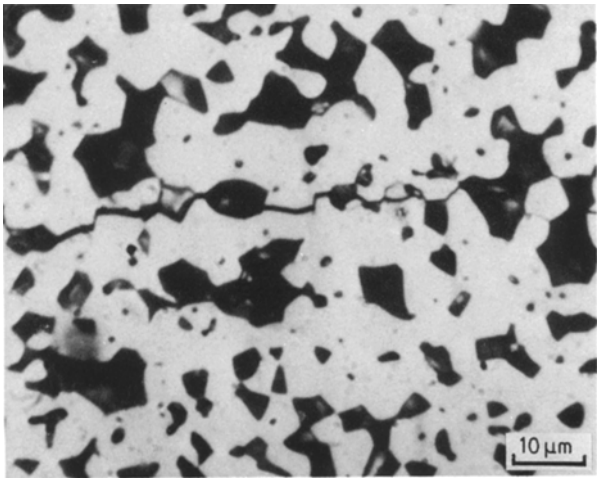

Figure 12 Radial crack from a Vickers indentation which is outside the field of view at left. Optical micrograph, reflected light. The dark grains are transparent ZrO_2. The fracture is mainly intergranular but passes through some of the ZrO_2 grains.

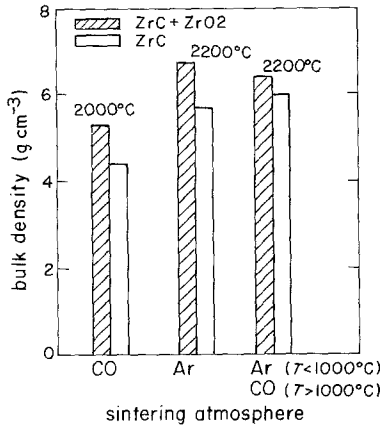

Figure 14 A comparison of the fired density obtained for pure ZrC and ZrC + 30% Type A ZrO_2 for different temperatures and different firing atmospheres. The ZrO_2 addition improved the density in every case.

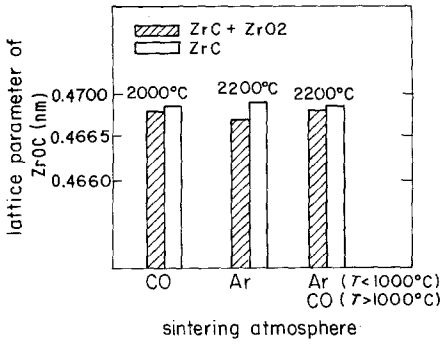

Figure 15 The lattice parameter of the oxicarbide phase resulting from the same sintering conditions shown in Fig. 14. The smaller lattice parameter in the oxicarbide from the ZrC–ZrO_2 mixtures indicates a higher oxygen content.

monoxide gas. The formation of the carbide surface layer did not occur in the carbon monoxide atmosphere, and the ZrO_2 phase remained intact. The resulting hardness values were higher than those obtained for specimens fired in flowing argon.

The presence of ZrO_2 clearly improved the sintering of the composite compared to pure ZrC. It was thought that the formation of a defect oxicarbide may be responsible for enhanced diffusion and densification in the ZrC and that the role of the ZrO_2 was as an oxygen source.

Attempts were made to sinter pure ZrC in a carbon monoxide atmosphere to provide a low but significant oxygen pressure to form a defect oxicarbide without the presence of ZrO_2. Fig. 14 compares the results in various atmospheres with and without ZrO_2 additions. In every case, the presence of ZrO_2 improved the sintered density. Fig. 15 shows that the presence of ZrO_2 resulted in a smaller lattice parameter for the oxicarbide product which is an indication of higher oxygen content.

4. Conclusions

Additions of 20 to 40 wt % yttira containing ZrO_2 enhances the sintering of ZrC. Specimens with green density of 55% and above, sintered to greater than 99% theoretical density in 1 h at 2000° C in argon in a carbon tube furnace. Green densities as low as 45% could be sintered to near theoretical density in 1 h at 2200° C. During heat treatment, the ZrC reacts with oxygen to form an oxicarbide of variable composition. The source of oxygen is from ZrO_2 which reacts with carbon in the system to also form oxicarbide. The final product was a composite of zirconium carbide and zirconium oxide.

The fracture toughness of pure ZrC was 4 MPa $m^{1/2}$ and increased for the composite to 5.8 MPa $m^{1/2}$ at 40 wt % ZrO_2. The four-point bend strength, which reached a maximum of 320 MPa at 40 wt % ZrO_2, was probably limited by singular processing flaws. The fracture path was irregular and mainly intergranular.

Acknowledgements

The authors thank the Sumitomo Cement Company, Central Research Laboratory for their financial support and Jean-Maurice Ferauge for his assistance in mechanical property testing and analysis.

References

1. L. E. TOTH, "Transition Metal Carbides and Nitrides" (Academic, New York, 1971).
2. D. W. LEE and J. S. HAGGERTY, *J. Amer. Ceram. Soc.* **52** (1969) 641.
3. R. DAROLIA and T. F. ARCHBOLD, *J. Mater. Sci.* **11** (1976) 283.
4. P. BARNIER, C. BRODHAG and F. THEVENOT, *ibid.* **21** (1986) 2547.
5. I. I. SPIVAK and V. V. KLIMENKO, *Sov. Powder Metall. Metal Ceram. (Poroshkovaya Metallurgiya)* **131** (1973) 24.
6. V. M. GROPYANOV and L. M. BEL'TYUKOVA, *ibid.* **67** (1967) 25.
7. V. P. BULYCHEV, R. A. ANDRIEVSKIL and L. B. NEXHEVENKO, *ibid.* **172** (1977) 38.
8. Sumitomo Cement Company, Central Research Laboratory, Chiba, Japan (1986).
9. R. V. SARA, *J. Amer. Ceram. Soc.* **48** (1965) 243.
10. S. K. SARKAR, A. D. MILLER and J. I. MUELLER, *ibid.* **55** (1972) 628.
11. G. K. BANSAL and W. H. DUCKWORTH, "Fracture Mechanics Applied to Brittle Materials", ASTM STP 678, edited by S. W. Freeman (American Society for Testing Materials, Philadelphia, Pennsylvania, 1979) p. 38.
12. T. WATANABE and K. SHOUBU, *J. Amer. Ceram. Soc.* **68** (1985) C-34.
13. R. P. WAHI and B. ILSCHNER, *J. Mater. Sci.* **15** (1980) 875.
14. F. F. LANGE, *J. Amer. Ceram. Soc.* **56** (1973) 445.
15. C. GRESKOVICH and J. A. PALM, *ibid.* **63** (1980) 597.
16. K. T. FABER and A. G. EVANS, *Commun. Amer. Ceram. Soc.* (1983) C-94.
17. G. C. WEI and P. F. BECHER, *J. Amer. Ceram. Soc.* **67** (1984) 571.

Received 22 August
and accepted 1 December 1987